Supplementary material: Convection in an Internally-Heated Stratified Heterogeneous Reservoir

A. Limare, C. Jaupart, E. Kaminski, L. Fourel, and C.G. Farnetani

Fluid parameters and experimental conditions for the heterogeneous experiments

Number	$\mu_2(Pa \cdot s)$	$\rho_2(kg \cdot m^{-3})$	$\frac{\Delta\rho}{\rho}(\%)$	$\alpha_2(K^{-1})$	$H(W \cdot m^{-3})$
1	0.670	999.6	0.42	$2.32\ 10^{-4}$	15540
2	1.834	1000.0	0.32	$2.47\ 10^{-4}$	15540
3	0.676	999.9	0.40	$2.30\ 10^{-4}$	15540
4	1.196	999.8	0.48	$2.31\ 10^{-4}$	15540
5	0.890	998.9	0.69	$2.31\ 10^{-4}$	15540
6	0.183	998.8	0.48	$2.37\ 10^{-4}$	15540
7	0.192	999.3	0.69	$2.20\ 10^{-4}$	15540
8	0.380	999.0	0.43	$2.38\ 10^{-4}$	7770
9	0.380	999.0	0.43	$2.38\ 10^{-4}$	3550
10	1.537	999.5	0.36	$2.46\ 10^{-4}$	3550
11	1.537	999.5	0.36	$2.46\ 10^{-4}$	7770
12	0.874	999.4	0.31	$2.35\ 10^{-4}$	7770
13	0.874	999.4	0.31	$2.35\ 10^{-4}$	3550
14	0.567	999.3	0.32	$2.37\ 10^{-4}$	3550
15	0.567	999.3	0.47	$2.37\ 10^{-4}$	7770
16	0.353	999.3	0.24	$2.32\ 10^{-4}$	3550
17	0.211	999.1	0.36	$2.33\ 10^{-4}$	3550
18	0.595	999.5	0.41	$2.28\ 10^{-4}$	7770
19	0.392	999.4	0.22	$2.30\ 10^{-4}$	11550
20	0.392	999.4	0.22	$2.30\ 10^{-4}$	15540
21	0.084	999.0	0.76	$2.19\ 10^{-4}$	22190
22	0.161	999.2	0.74	$2.20\ 10^{-4}$	22190
23	0.161	999.2	0.61	$2.20\ 10^{-4}$	11550
24	0.024	998.5	0.93	$2.30\ 10^{-4}$	22190
25	0.020	998.3	0.94	$2.30\ 10^{-4}$	22190
26	0.032	998.2	0.64	$2.26\ 10^{-4}$	22190
27	1.730	1000.0	0.28	$2.32\ 10^{-4}$	7770
28	0.006	998.4	0.93	$2.18\ 10^{-4}$	22190
29	0.006	998.4	0.93	$2.18\ 10^{-4}$	24430
30	0.047	998.6	0.74	$2.22\ 10^{-4}$	22210
31	0.044	998.6	0.74	$2.22\ 10^{-4}$	22210
32	0.015	997.9	0.79	$2.42\ 10^{-4}$	22215
33	0.015	997.9	0.79	$2.42\ 10^{-4}$	24408
34	0.004	997.8	1.44	$2.46\ 10^{-4}$	38886
35	0.004	997.5	1.44	$2.48\ 10^{-4}$	38886
36	0.408	999.1	0.25	$2.46\ 10^{-4}$	11541
37	0.387	998.0	0.25	$2.56\ 10^{-4}$	7770
38	0.019	998.0	1.13	$2.52\ 10^{-4}$	38886

Table S1: Fluid parameters and experimental conditions. The other parameters entering the Rayleigh-Roberts number are the thermal diffusivity and the thermal conductivity that are, for these type of samples, the ones of water ($1.46\ 10^{-7} m^2 s^{-1}$ and $0.6\ Wm^{-1}K^{-1}$, respectively).

Results for the steady-state volume-averaged temperature in homogeneous experiments

ΔT_H (K)	Ra_H	ΔT_{vol} ($^\circ C$)
94	5.01×10^4	14.73
142	8.22×10^4	20.30
148	9.17×10^4	23.67
72	1.03×10^5	10.54
114	1.48×10^5	15.70
81	2.99×10^5	9.55
154	3.05×10^5	22.25
167	3.47×10^5	25.90
75	4.02×10^5	10.29
83	4.21×10^5	10.14
94	6.58×10^5	10.07
94	6.69×10^5	10.16
144	1.07×10^6	13.26
136	1.11×10^6	14.17
131	1.32×10^6	13.09
57	1.44×10^6	6.18
248	2.47×10^6	18.3
153	2.50×10^6	13.24
145	3.05×10^6	11.78
170	3.13×10^6	14.50
94	3.14×10^6	7.50
100	3.34×10^6	9.01
131	4.01×10^6	12.11
108	4.04×10^6	8.62
141	4.88×10^6	9.66
150	5.62×10^6	8.97
126	6.04×10^6	9.91
138	7.18×10^6	8.71
249	1.04×10^7	15.51
256	1.47×10^7	15.56

Table S2: List of homogeneous experiments and their steady-state volume-averaged temperature (from Limare *et al.* (2015)).

Example of high B_{eff} and a low Ra_H for the time evolution of the dimensionless flux and the mean temperature

Figure S1 shows the evolution in time of the dimensionless flux and the mean temperature for an experiment with a high B_{eff} and a low Ra_H (experiment 10) together with the best-fit exponential function (black curves) and predictions of the simple theoretical model (red, dashed lines). Differences between the experimental data and the theoretical results are larger than for experiments at larger values of Ra_H. This is expected because the heat flux scaling laws with power-law exponent $\beta = -1/4$ are only valid for Ra_H values that are larger than about $> 6 \cdot 10^5$) (Limare *et al.*, 2015; Vilella *et al.*, 2018), such that the dynamics of the thin unstable thermal boundary layer are determined locally, independently of the bulk fluid layer. Differences between the data and predictions account for the fact that values of time constant τ_e and average temperature T_{vol} deviate slightly from the scaling laws, contributing to scatter in Figures 5 and 6.

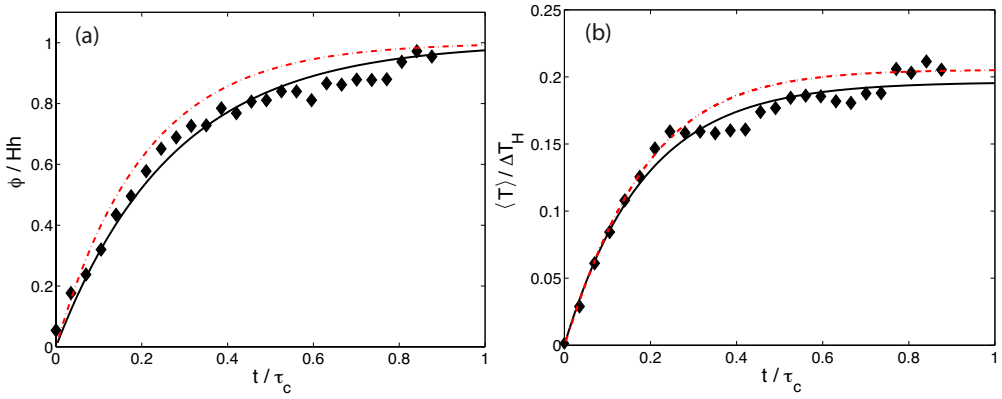

Figure S1: Dimensionless heat flux (c) and volume-averaged temperature (d) as a function of time normalised to the conduction time for the whole layer, $\tau_c = h^2/\kappa$, for experiment 10 (stratified regime, B_{cond}=2.7, Ra_H=3.4 10^4). Black diamonds represent experimental data, black lines represent exponential fits and red, dashed lines represent the results of transient calculations from equations 4.3 and 4.5.

Lower layer detection: threshold influence

The tank was first completely filled with the upper fluid and then the denser lower layer was injected at the bottom whilst the excess upper fluid was removed and weighted. The threshold composition value was chosen such that the initial value of the lower layer volume corresponded to the known injected volume. We explain in the text that the tearing out of thin shlieren of lower fluid generates a volume of mixed fluid adjacent to undiluted lower fluid, which shows up as the smearing of the interface. We are interested in the volume of undiluted or unmixed fluid and hence use the same threshold intensity value throughout. Figure S2 shows histograms of intensity levels in the tank (obtained from the individual pixel values) at several times. The two fluids are well separated and the threshold value selected is indicated by the dashed line, with the lower fluid identified by intensity values above the threshold. The volume estimate can be deduced directly from the cumulative distribution function (Figure R3). Small variations of the threshold intensity value have a weak impact on the volume estimate (which is given by the intersection of the CDF curve with the threshold value). This figure has been added to the Supplementary Material.

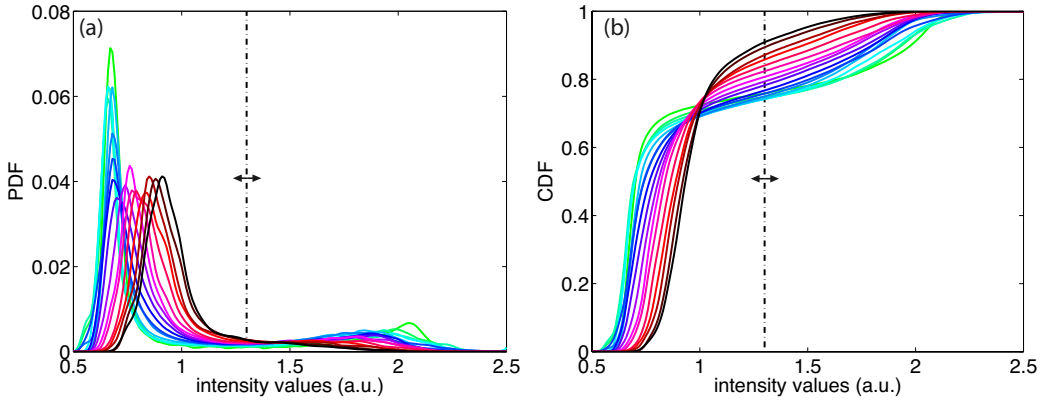

Figure S2: Probability density function (a) and cumulative density function (b) of the "composition" image for experiment 7. Colors indicate time evolution from green to blue, red and black. The dashed line indicate the threshold value used in Figure 19.

Adiabatic lower boundary

The tank is made of PMMA whose density and specific heat are ρ=1200 kgm^{-3} and 1500 $Jkg^{-1}K^{-1}$ respectively. The bottom wall (thickness h_w=10mm) of the tank has to heat up and follows the temperature at the bottom of the fluid. Let's consider the example in Figure 3 (experiment 21): the bottom wall temperature increase is at most ΔT=7°C in δt=40min. The heat flux in this transient period is $\rho C_p h_w \Delta T/\delta t$ =52 $W\ m^{-2}$, which represents 5% of the steady-state heat flux (1110 Wm^{-2}), therefore we can consider this boundary condition as adiabatic.

References

Limare, A., Vilella, K., Di Giuseppe, E., Farnetani, C., Kaminski, E., Surducan, E., V., Surducan, Neamtu, C., Fourel, L. & Jaupart, C. 2015 Microwave-heating laboratory experiments for planetary mantle convection. *Journal of Fluid Mechanics* **1565**, 14–18.

Vilella, K., Limare, A., Jaupart, C., Farnetani, C., Fourel, L. & Kaminski, E. 2018 Fundamentals of laminar free convection in internally heated fluids at values of the Rayleigh-Roberts number up to 10^9. *Journal of Fluid Mechanics* **846**, 966–998.